Carbohydrate Polymers 84 (2011) 631–637

Contents lists available at ScienceDirect

Carbohydrate Polymers

journal homepage: www.elsevier.com/locate/carbpol

Studies on the properties of graphene oxide-reinforced starch biocomposites

Rui Li, Changhua Liu*, Jun Ma

College of Chemistry and Chemical Engineering, Southwest University, Chongqing 400715, PR China

ARTICLE INFO

Article history:
Received 3 November 2010
Received in revised form
10 December 2010
Accepted 13 December 2010
Available online 21 December 2010

Keywords:
Starch
Graphene oxide
Biocomposite films
Interaction
Properties

ABSTRACT

Glycerol-plasticized pea starch/graphene oxide (PS/GO-n) biocomposite films with different loading levels of graphene oxide (GO) were prepared by solution casting method. The structure, morphologies and properties of biocomposite films were characterized by Fourier transform infrared (FTIR) spectroscopy, X-ray diffraction (XRD), atomic force microscopy (AFM), thermal gravimetric analysis (TGA), Ultraviolet–visible (UV–vis) and tensile tests. The results revealed that hydrogen bonding formed in the biocomposite films, which improved compatibility between GO fillers and starch matrix. The tensile strength (σ_b) and Young's modulus (E) of starch films containing 2.0 wt% GO increased from 4.56 MPa, 0.11 GPa to 13.79 MPa, 1.05 GPa, respectively, while the elongation at break (ε_b) decreased from 36.06% to 12.11%. The introduction of GO also reduced moisture uptake (Mu) and UV transmittance of starch films. In addition, TGA showed that the thermal stability of biocomposite films was better than that of neat starch film.

1. Introduction

Polymer composites are of scientific and industrial interest because of their enhanced properties arising from the reinforcement of nanofillers (Avella et al., 2005; Chung et al., 2010; Huang, Yu, & Ma, 2004). Recently, graphene, with one-atom-thick two-dimensional individual sheet structure composed of sp^2-hybridized carbon, has attracted a great deal of attention due to its unique structure and properties (Geim & Novoselov, 2007). It combines the lower price and the layered structure of clays with the superior thermal and electrical properties of carbon nanotubes. So graphene can be used as an alternative to make polymer composites with competitive multifunctional properties (Jiang, Shen, Wu, & Shen, 2010; Kim & Macosko, 2009; Wei et al., 2009). However, it is well known that the interfacial interaction is crucial to improve the properties of polymer, while as-prepared graphene cannot be dispersed in water or organic solvent. Therefore, graphene oxide (GO) was explored as a promising filler to synthesize polymer/GO composites. Compared with graphene, GO is hydrophilic and can form strong physical interactions with polymer due to various oxygen functional groups including hydroxyls, epoxides, carbonyls and carboxyls. Meanwhile, GO sheets can be intercalated or exfoliated by small molecules or polymers (Liu, Gong, Xiao, & Xiao, 2000; Matsuo, Tahara, & Sugie, 1997). In addition, some authors have reported that the thermal stability, electrical and mechanical properties of polymers could be greatly improved by the incorporation of GO nanosheets (Kai, Hirota, Hua, & Inoue, 2008; Wu et al., 2008; Xu et al., 2001).

Based on the above facts, we choose pea starch (PS) as matrix because water can be used as the common solvent, resulting in well-dispersed GO in polymer matrix. It is well known that starch is one of the best candidates for replacing current synthetic plastics due to its attractive combination of biodegradability, low cost, abundance and renewable (Avella et al., 2005; Chung et al., 2010; Geim & Novoselov, 2007; Huang et al., 2004). It has been applied in the field of agriculture, medicine, and packaging industries (Guan, Eskridge, & Hanna, 2005; Ou, Li, & Yang, 2001; Rehman & Shah, 2005). Unfortunately, the starch-based biocomposites exhibit many disadvantages (e.g. strong hydrophilic character, poor mechanical properties, low thermal stability) compared to conventional polymers (Wilhelma, Sierakowski, Souza, & Wypychc, 2003), which make it unsatisfactory for practical applications. Therefore, we expect that the properties of starch films can be improved by the incorporation of graphene oxide.

A series of PS/GO-n biocomposite films were prepared by solution casting method. The aim of this work is to study the influence of GO loading on the morphologic, thermal stability, mechanical properties and moisture uptake of plasticized pea starch films. The biocomposites were analyzed by Fourier transform infrared (FTIR), X-ray diffraction (XRD), atomic force microscopy (AFM), thermal gravimetric analysis (TGA) and tensile tests. The fundamental structure–property relationship of GO-based starch biocomposites was also discussed.

* Corresponding author. Tel.: +86 2368252360; fax: +86 2368254000.
E-mail address: chliu@swu.edu.cn (C. Liu).

0144-8617/$ – see front matter © 2010 Elsevier Ltd. All rights reserved.
doi:10.1016/j.carbpol.2010.12.041

2. Experimental

2.1. Materials

Pea starch (PS), with an average granule size of 29 μm and composed of 35% amylose and 65% amylopectin, was provided by Nutri-Pea Limited (Portage la Prairie, Manitoba, Canada). The plasticizer, glycerol (99%), was purchased from Maoye Chemical Company (Chongqing, China). Graphite powder was supplied by Shanghai Huayi Group Hua Yuan Chemical Company Limited (Shanghai, China). Potassium persulfate ($K_2S_2O_8$), phosphorus (V) oxide (P_2O_5) and hydrogen peroxide 30% (H_2O_2, 30%) were supplied by Chengdu Kelong Chemical Reagent Company (Chengdu, China). Sulfuric acid and hydrochloric acid were purchased from Chongqing Chuandong Chemical Reagent Factory (Chongqing, China). The water used was distilled and deionized.

2.2. Preparation of GO

Graphene oxide was prepared from natural graphite by the well-known Hummers method (William, Hummers, & Richard, 1958). In brief, 2 g natural graphite powder, 1 g $NaNO_3$ and 46 mL H_2SO_4 were added into a 250 mL beaker sequentially under stirring in an ice-bath. Next, 6 g $KMnO_4$ was added slowly into the beaker under stirring and the temperature was controlled below 20 °C. The ice-bath was then removed and the system was heated at 35 °C. At the end of 30 min, 92 mL water was added slowly into the system and it was stirred for another 15 min. Then 280 mL hot water with 60 °C and 3% H_2O_2 aqueous solution were added to reduce the residual $KMnO_4$ till no bubble was appeared. Finally, the solution was filtered resulting in a yellow-brown filter cake, which was washed by warm water until the pH value of the upper layer suspension arrives at near 7. Graphene oxide powder was obtained under vacuum for 48 h at 50 °C.

2.3. Preparation of PS/GO-n biocomposite films

The procedures for preparing glycerol-plasticized pea starch/graphene oxide (PS/GO-n) biocomposite films were described as follows: GO was re-dispersed in 70 mL of water and treated with ultrasound for 1.5 h to make a homogeneous brown dispersion. The GO fillers loading level (0, 0.4, 0.8, 1.0, 1.5 and 2.0 wt%) was based on the amount of pea starch. Then 2 g PS powder and 0.5 g glycerol were added to this solution ultrasound for another 30 min. After that, the mixture was heated at 95 °C for 0.5 h with constant stirring in order to plasticize the pea starch, followed by stirring at 60 °C for 0.5 h. After degassing under vacuum, the PS/GO solution was poured into a glass plate and heated at 50 °C to obtain dry films. A series of biocomposite films were prepared and respectively coded as PS, PS/GO-1, PS/GO-2, PS/GO-3, PS/GO-4 and PS/GO-5, where the number represented the different GO loadings.

2.4. Characterization of the biocomposite films

Fourier transform infrared (FTIR) spectra of GO and the blend films were recorded on a Nicolet (Madison, WI, USA) 170SX Fourier transform infrared spectrometer in the wavelength range of 4000–500 cm^{-1} in the attenuated total reflection mode.

X-ray diffraction (XRD) patterns of the samples were recorded on an X-ray diffractometer (XRD-3D, PuXi, Beijing, China) at a voltage of 36 kV and a current of 20 mA using Cu $K\alpha$ radiation ($\lambda = 0.154$ nm). The scanning rate was 4°/min and the scanning scope of 2θ was 3–50° at room temperature.

The surface morphologies and roughness of the prepared biocomposites were observed by atomic force microscopy (AFM) (Vecco Instruments, Inc., New York) in the tapping mode. The film surfaces were imaged in a scan size of 3 μm × 3 μm.

Thermogravimetric analysis (TGA) of the PS and PS/GO-n biocomposite films was performed using a TA-STDQ600 (TA Instruments Inc., New Castle, USA). The thermogram curves were acquired between 25 °C and 500 °C at a heating rate of 10 °C/min. The experiment was carried out in nitrogen environment using a flow rate 20 mL/min in order to avoid thermoxidative degradation. An empty pan was used as a reference.

The Ultraviolet–visible (UV–vis) spectra of the PS/GO-n biocomposites were recorded from 200 to 800 nm using a UV–vis spectrophotometer 2550 (Suzhou Instruments Manufacture Co., Ltd.).

The tensile strength (σ_b), Young's modulus (E) and elongation at break (ε_b) of the samples were tested using a Micro-electronics Universal Testing Instrument Model Sans 6500 (Shenzhen Sans Testing Machine Co. Ltd., Shenzhen, China) with the cross-head speed was 10 mm/min. According to the Chinese standard method (GB 13022-91), all the films were cut into 10 mm × 100 mm (width × length) strips and mounted between cardboard grips (150 mm × 300 mm) using adhesive so that the final area exposed was 10 mm × 50 mm. Before testing, the samples were equilibrated at 43% *RH* (relative humidity) for more than one week at room temperature. The average value of σ_b, E and ε_b was set as the representative value.

The moisture uptake of the PS/GO-n biocomposite films was determined. The samples used were thin rectangular strips with dimensions of 50 mm × 10 mm × 0.1 mm. The initial weight of dry biocomposite films was determined by drying to constant weight in an oven at 80 °C, after weighing, they were equilibrated at 98% *RH*. The samples were removed at desired intervals and weighed until the equilibrium state was reached. The moisture uptake (Mu) of the samples was calculated as follows:

$$Mu\,(\%) = \frac{W_1 - W_0}{W_0} \times 100 \quad (1)$$

where W_0 and W_1 were the weight of the sample before exposure to 98% *RH* and after equilibrium, respectively. Each moisture uptake experiment was repeated three times, and the average values were reported.

3. Results and discussion

3.1. Fourier transform infrared spectroscopy

As seen from Fig. 1, the FTIR spectrum of GO showed a broad band at 3430 cm^{-1}, which was related to the OH groups, and bands at 1720 cm^{-1}, 1628 cm^{-1}, which were typical of carboxyl and carbonyl groups (Wang et al., 2009). Besides, other C–O functionalities such as C–OH (1400 cm^{-1}), C–O–C (1134 cm^{-1}) and C–O (1059 cm^{-1}) were also clearly visible (Chandra, Sahu, & Pramanik, 2010). These main characteristic peaks indicated that GO had been synthesized successfully.

For neat starch film, the stretching and bending vibration of –OH groups occurred at 3283 cm^{-1} and 1650 cm^{-1}, respectively. The bands at 1151 cm^{-1} and 1077 cm^{-1} were attributed to the stretching vibration of C–O in C–O–H groups and the band at 997 cm^{-1} was attributed to the stretching vibration of C–O in C–O–C groups (Chen, Cao, Chang, & Huneault, 2008). The peak at 2928 cm^{-1} was characteristic of the C–H stretching associated with ring methane hydrogen atoms (Ma, Chang, Yang, & Yu, 2009). Meanwhile, the characteristic peak of C–O–C ring vibration in starch located at 765 cm^{-1} (Chen et al., 2008). After the formation of PS/GO-5 biocomposite films, the characteristic peaks at 1650, 1151, 1077 and 997 cm^{-1} of PS shifted to lower wave-numbers 1642, 1145, 1072 and 993 cm^{-1}, respectively. This indicated that hydrogen bonding between GO and PS formed in the biocomposite films.

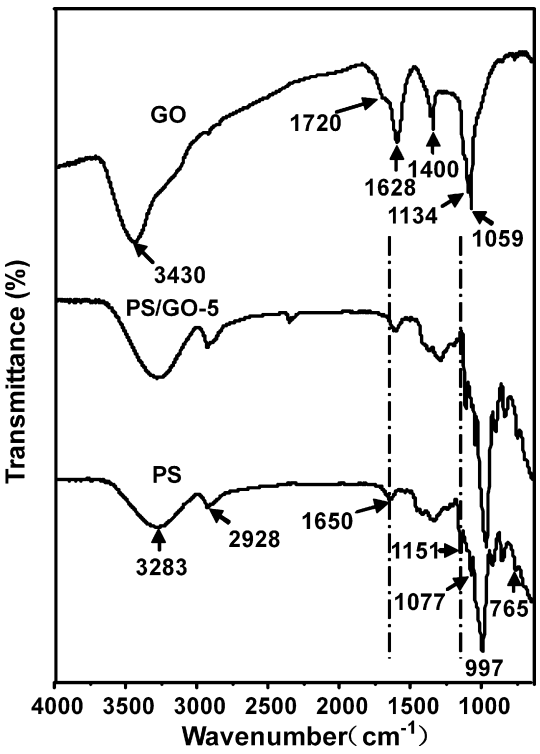

Fig. 1. FTIR spectra of GO powder, PS and PS/GO-5 biocomposite films.

3.2. X-ray diffraction

The XRD patterns of the films with different loadings of graphene oxide are shown in Fig. 2. The interlayer spacing of our synthesized graphene oxide was 0.80 nm ($2\theta = 11.1^\circ$), which was similar to the previous report (Han, Yan, Chen, & Li, 2010). For neat starch film, it had the typical C-type crystalline pattern containing A-type and B-type polymorphs like other legume starches (Hoover & Ratnayake, 2002; Ratnayake, Hoover, & Warkentin, 2002), which exhibited five main diffraction peaks at 5.7° (characteristic of B type polymorphs), 15.1° (characteristic of A type polymorphs), 17.1° (characteristic of both A and B type polymorphs), 19.9° and 22.1° (characteristic of B type polymorphs) (Wang, Yu, & Gao, 2005). After adding graphene oxide, the characteristic diffraction peak of graphite oxide was not observed, while the diffraction intensity of PS film decreased. This result indicated that GO sheets were well exfoliated and uniformly dispersed in PS matrix and the crystalline structure of PS was affected by the incorporation of GO component (Xu, Hong, Bai, Li, & Shi, 2009). The reason might be that, in the gelation processing, the small size of GO easily entered into starch chains and formed hydrogen bonding with PS, which restricted the mobility of polymer chains and led to a considerable slowing down of the re-crystallization of PS.

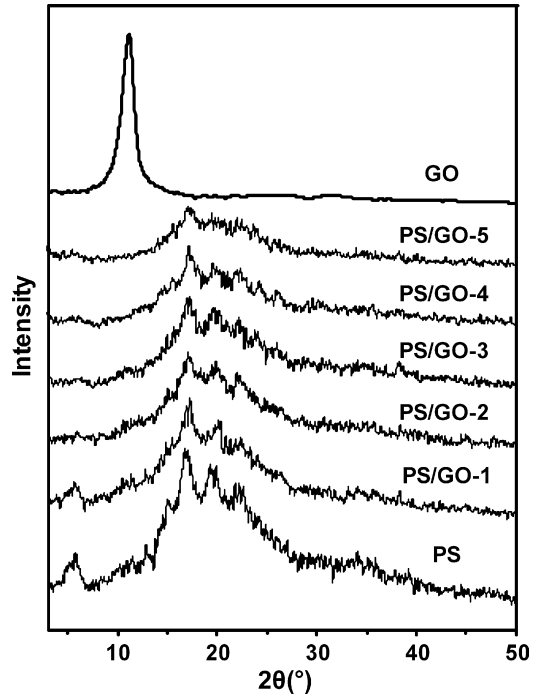

Fig. 2. XRD patterns of GO powder and PS/GO-n biocomposite films.

3.3. Morphological image analysis

The morphologies of as-synthesized materials are studied by TEM and AFM. As shown in Fig. 3(a), the GO nanosheets appeared flat and transparent, with some wrinkles and folding on the surface and edge. Corrugation and scrolling are part of the intrinsic nature of graphene nanosheets, which result from the fact that the 2-D membrane structure becomes thermodynamically stable via bending (Meyer et al., 2007).

Furthermore, to observe the surfaces of PS and blend films, the AFM images over a scan area of 3 μm × 3 μm are also displayed in Fig. 3. It was found that the surface morphologies of PS/GO-n biocomposites were different from neat PS film. The surface roughness parameters of PS/GO-3 films (Fig. 3(c)), such as the mean roughness (R_a = 7.330 nm) and the root mean square of the Z data (R_q = 10.082 nm) (Khulbe, Kruczek, Chowdhury, Cacne, & Matsuura, 1996), were lower than that of neat PS film (Fig. 3(b), R_a = 8.068 nm, R_q = 10.500 nm). The results suggested that the compatibility between GO and starch was good, and the GO fillers were dispersed uniformly in starch matrix. This could be attributed to plenty of oxygen functional groups on the surface of GO, which were easy to form strong hydrogen bonding with starch molecules. However, when GO loading was 2.0 wt%, the blisters and depressions could be observed on the surface of PS/GO-5 film (Fig. 3(d)), resulting in a higher roughness (R_a = 14.009 nm, R_q = 17.926 nm). The difference of microstructure was presumably due to the poor dispersion and aggregations of GO at high loading.

3.4. UV–vis

Transparency may be affected by various factors, including film thickness, fortunately, there was an insignificant difference in the average thickness of the film samples. Fig. 4 shows the UV–vis percent transmittance values of PS/GO-n biocomposites with different levels of GO loading. It was found that the UV transmittance decreased with increasing GO content. In the UV range (290–400 nm) neat PS had very high transmittance, while the transmittance of UV light for PS/GO-5 was nearly 0%, meaning that most of UV light was shielded. The PS/GO-n biocomposite films might effectively protect against UV light, and could potentially be applied to UV-shielding materials.

3.5. Thermal stability analysis

Thermal analysis was performed in order to determine if the addition of GO could produce any change on the thermal decomposition behavior of starch. The thermogravimetric (TG) and derivative thermogravimetric (DTG) curves of the PS film and PS/GO-n biocomposites are shown in Fig. 5(a) and (b), respectively. It could be noted basically two main thermal events. The

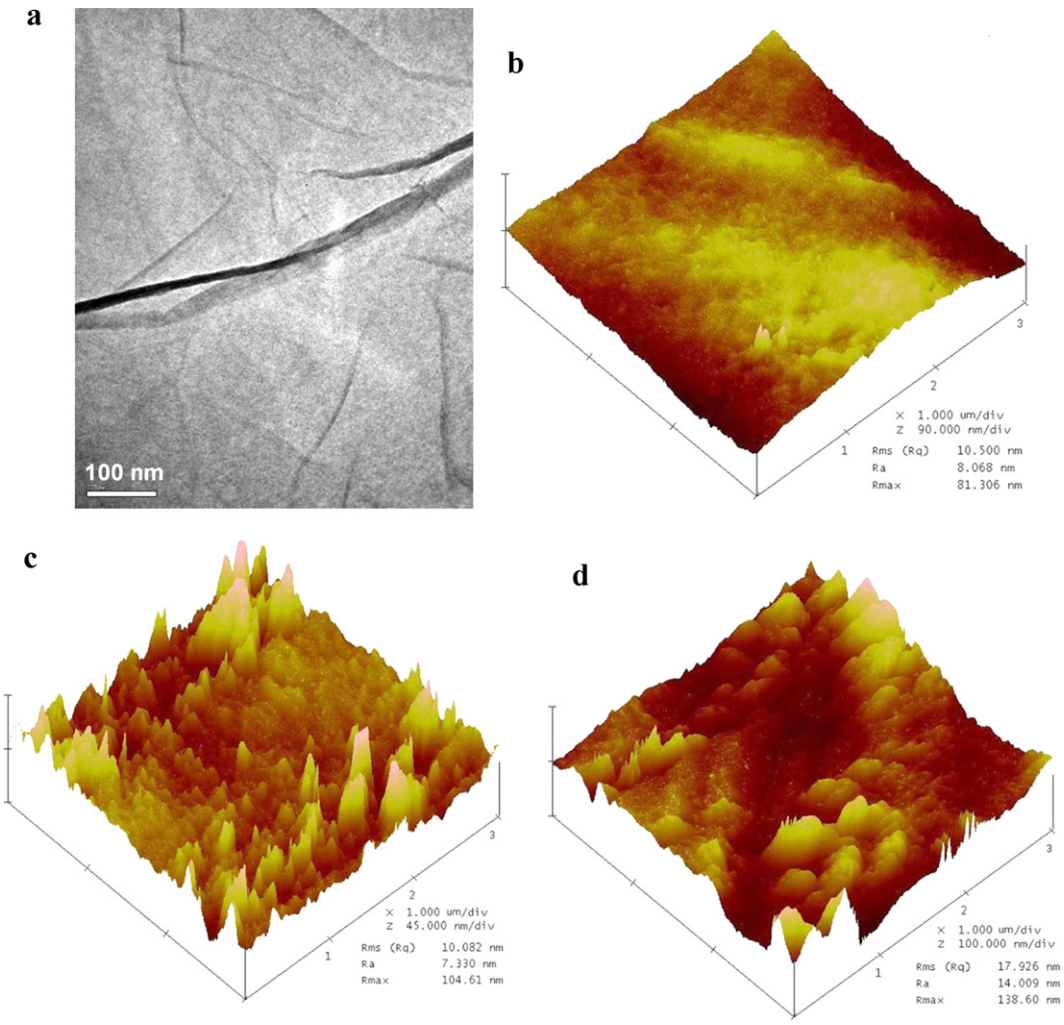

Fig. 3. TEM image of GO powder (a), AFM images of PS (b), PS/GO-3 (c) and PS/GO-5 (d) biocomposite films.

first one before 100 °C was attributed to the elimination of the water absorbed by starch (Schlemmer, Angélica, & Sales, 2010). The second stage of the weight loss in the temperature range of 250–350 °C corresponded to decomposition of starch (Ma, Chang, Yu, & Stumborg, 2009; Schlemmer et al., 2010). An improvement in the thermal stability of the biocomposite films could be seen with an increase of the fillers loading. For example, the decomposed residual weight of PS/GO-n films increased as the GO loading increased. Meanwhile, all experimental results of TGA and DTG, which was generally accepted and used to assess a material's lifetime, are listed in Table 1. Such as the initial decomposed temperature (IDT), the final decomposed temperature (FDT) (Khurana, Aggarwal, Narula1, & Choudhary, 2003), the integral procedural decomposition temperature (IPDT) (Park & Kim, 2001), the temperature at 50% weight loss ($T_{-50\%}$) and the temperature at the maximum rate of mass loss (T_{max}). It could be observed that all PS/GO-n biocomposite films showed a higher decomposition temperature than neat PS film. These results indicated that the decomposition temperatures of starch increased by the addition of GO. The reason might be that the mobility of PS chains

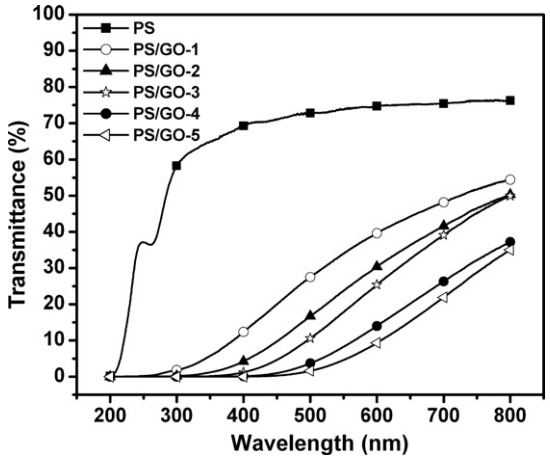

Fig. 4. UV–vis transmittance of PS and PS/GO-n biocomposite films.

Table 1
Thermal properties of neat PS and PS/GO-n biocomposite films.

Sample	IDT (°C)[a]	FDT (°C)[b]	IPDT (°C)[c]	$T_{-50\%}$ (°C)[d]	T_{max} (°C)[e]
PS	284.2	326.9	177.3	273.8	311.5
PS/GO-1	291.6	333.7	222.4	292.7	318.2
PS/GO-3	295.3	332.6	244.1	298.0	319.3
PS/GO-5	294.4	334.3	251.6	294.6	318.4

[a] The initial decomposed temperature.
[b] The final decomposed temperature.
[c] The integral procedural decomposition temperature.
[d] The temperature at 50% weight loss.
[e] The temperature at the maximum rate of mass loss.

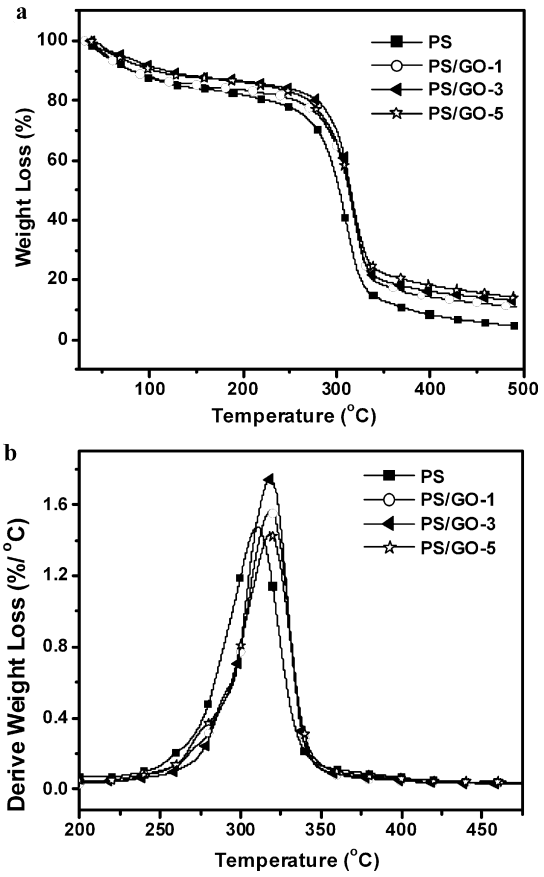

Fig. 5. TG (a) and DTG (b) curves of PS and PS/GO-n biocomposite films.

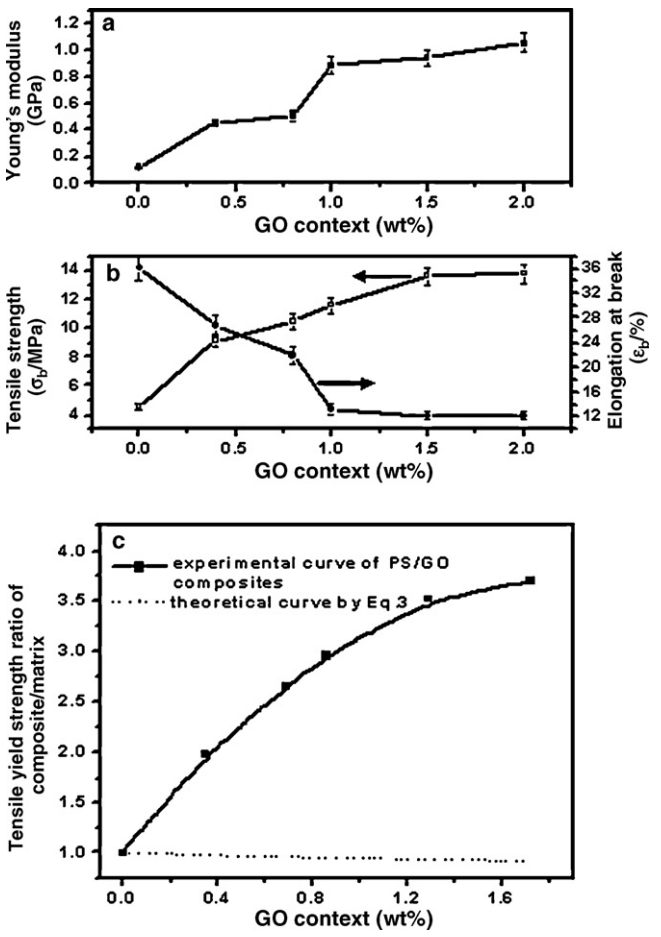

Fig. 6. Effect of GO weight fraction on Young's modulus (a), tensile strength and elongation at break (b) of PS/GO biocomposite films; effect of GO volume fraction on tensile yield strength ratio of PS/GO biocomposite films (c).

was suppressed by strong hydrogen bonding interactions with GO.

3.6. Mechanical properties

The effect of GO loading on the mechanical properties of starch films is shown in Fig. 6(a) and (b). As GO loading increased, both the tensile strength (σ_b) and Young's modulus (E) increased, but the elongation at break (ε_b) of the biocomposites decreased. When GO loading varied from 0 to 2.0 wt%, the σ_b and E increased from 4.56 MPa, 0.11 GPa to 13.79 MPa, 1.05 GPa, respectively, while ε_b decreased from 36.06% to 12.11%. These results suggested that GO could improve the strength and stiffness of starch films at the expense of flexibility, which was similar to previous reports about starch/nanofiller (Ma, Yu, & Wang, 2008; Yu, Yang, Liu, & Ma, 2009). The improvement in the mechanical properties was due to the good dispersion of GO within the starch matrix and the strong interfacial interactions between GO and PS matrix. In consequence, when the biocomposites were under tensile stress, the fillers were difficult to disconnect from the matrix, and could resist and transfer the imposed force, leading to weaken the loading stresses of starch matrix. But the good dispersion of GO in PS matrix also restrained the slippage movement among starch molecules, so adding GO significantly decreased elongation at break of PS film.

In addition, interfacial interaction between the fillers and matrix was an important factor affecting the mechanical properties of the composites. Thus, theoretical tensile yield strength of the composites was modeled for the cases of adhesion and no adhesion between the filler particles and matrix. In the case of no adhesion, the interfacial layer could not transfer stress. The tensile yield strengths of the composites could be predicted using Nicholais–Narkis models, Eq. (2) (Metin et al., 2004).

$$\sigma_c = \sigma_m(1 - a\Phi_f^b) \tag{2}$$

where Φ_f, σ_c and σ_m were volume fraction of filler, and tensile yield strengths of the composite and matrix, respectively. In the Nicholais and Narkis model, parameters a and b were the constants related to filler–matrix interaction and geometry of the filler, respectively. The value (a) of less than 1.21 represented good adhesion for composites containing spherical fillers. In the absence of adhesion for the composites, Eq. (2) became

$$\frac{\sigma_c}{\sigma_m} = (1 - 1.21\Phi_f^{2/3}) \tag{3}$$

This model was based on the assumption that the decrease of tensile strength was due to the reduction in effective cross-section area caused by the spherical filler particles. If perfect adhesion was present between PS and GO particles, the loading stresses would be transferred to the GO, and no reduction in effective surface area would result.

The densities of PS and GO were 1.15 g/cm^3 and 1.02 g/cm^3, respectively. The weight fraction of filler was transferred to volume fraction. The experimental and theoretical curves are plotted in Fig. 6(c). The experimental values of PS/GO-n composites were much higher than that calculated by Eq. (3). This indicated that there was the remarkable adhesion between PS matrix and GO fillers. This result also proved that the strong hydrogen bonding formed in the PS/GO-n biocomposite films.

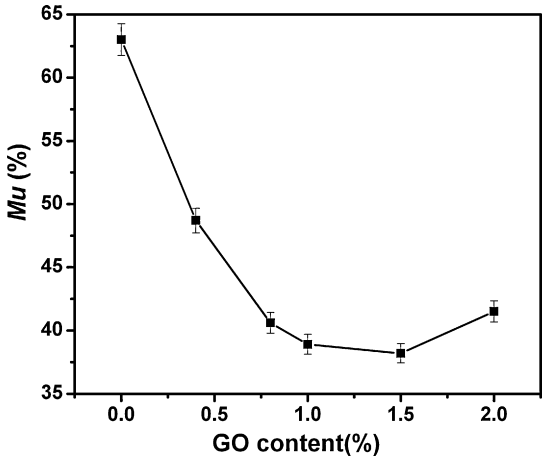

Fig. 7. The values of *Mu* at equilibrium of PS and PS/GO-n biocomposite films.

3.7. Moisture uptake of the films

Moisture sensitivity of starch-based material is a key challenge towards the substitution of traditional plastics for commodity, most precisely, for packaging applications. So the moisture uptake (*Mu*) of the films at 98% *RH* is tested and the results are given in Fig. 7. It was observed that the values of *Mu* for PS/GO-n biocomposites were lower than that of neat PS. When GO loading reached 1.5 wt%, the biocomposite films showed the lowest moisture uptake value (38.2%). These results indicated that the addition of GO improved the water resistance of the starch films. The reason could be that the GO was able to form hydrogen bonding with starch and these strong interactions could reduce the diffusion of water molecules in the material. Furthermore, the GO produced a tortuous pathway and also a diminution of the length of free way for water uptake. Similar results were obtained by other authors (Almasi, Ghanbarzadeha, & Entezami, 2010; Cyras, Manfredi, Ton-That, & Vázquez, 2008).

4. Conclusion

In this paper, the high-performance PS/GO-n composite films have been successfully prepared. The structures and properties of composite films were strongly depended on the interfacial interaction and GO loading. In view of the results from the FTIR, the strong hydrogen bonding formed between PS and GO, resulting in better compatibility between them. Results from AFM showed that the fillers were dispersed well when GO loading was lower, but the aggregations formed when adding higher loading of GO into starch. Tensile testing showed that the incorporation of GO could improve the strength and stiffness of starch films at the expensive of the flexibility. When GO loading was 2.0 wt%, the tensile strength and Young's modulus of the biocomposite films were about 3 times and 10 times higher than that of neat starch film, respectively. But the elongation at break decreased from 36.06% to 12.11%. Meantime, TGA and *Mu* studies showed the PS/GO-n composite films exhibited higher thermal stability and better moisture barrier property than neat starch. In addition, the results from the UV–vis showed that the PS/GO-n films could effectively protect against UV light. Therefore, the starch biocomposites will have promising applications as UV-shielding packing materials.

References

Almasi, H., Ghanbarzadeha, B., & Entezami, A. A. (2010). Physicochemical properties of starch–CMC–nanoclay biodegradable films. *International Journal of Biological Macromolecules*, *46*, 1–5.

Avella, M., Vlieger, J. J. D., Errico, M. E., Fischer, S., Vacca, P., & Volpe, M. G. (2005). Biodegradable starch/clay nanocomposite films for food packaging applications. *Food Chemistry*, *93*, 467–474.

Chandra, S., Sahu, S., & Pramanik, P. (2010). A novel synthesis of graphene by dichromate oxidation. *Materials Science and Engineering B*, *167*, 133–136.

Chen, Y., Cao, X. D., Chang, P. R., & Huneault, M. A. (2008). Comparative study on the films of poly(vinyl alcohol)/pea starch nanocrystals and poly(vinyl alcohol)/native pea starch. *Carbohydrate Polymers*, *73*, 8–17.

Chung, Y. L., Ansari, S., Estevez, L., Hayrapetyan, S., Giannelis, E. P., & Lai, H. M. (2010). Preparation and properties of biodegradable starch–clay nanocomposites. *Carbohydrate Polymers*, *79*, 391–396.

Cyras, V. P., Manfredi, L. B., Ton-That, M. T., & Vázquez, A. (2008). Physical and mechanical properties of thermoplastic starch/montmorillonite nanocomposite films. *Carbohydrate Polymers*, *73*, 55–63.

Geim, A. K., & Novoselov, K. S. (2007). The rise of graphene. *Nature Materials*, *6*, 183–191.

Guan, J. J., Eskridge, K. M., & Hanna, M. A. (2005). Acetylated starch–polylactic acid loose-fill packaging materials. *Industrial Crops and Products*, *22*, 109–123.

Han, D. L., Yan, L. F., Chen, W. F., & Li, W. (2010). Preparation of chitosan/graphene oxide composite film with enhanced mechanical strength in the wet state. *Carbohydrate Polymers*, doi:10.1016/j.carbpol.2010.08.038

Hoover, R., & Ratnayake, W. S. (2002). Starch characteristics of black bean, chick pea, lentil, navy bean and pinto bean cultivars grown in Canada. *Food Chemistry*, *78*, 489–498.

Huang, M. F., Yu, J. G., & Ma, X. F. (2004). Studies on the properties of montmorillonite-reinforced thermoplastic starch composites. *Polymer*, *45*, 7017–7023.

Jiang, L., Shen, X. P., Wu, J. L., & Shen, K. C. (2010). Preparation and characterization of graphene/poly(vinyl alcohol). *Nanocomposites*, *118*, 275–279.

Kai, W. H., Hirota, Y., Hua, L., & Inoue, Y. (2008). Thermal and mechanical properties of a poly(epsilon-caprolactone)/graphite oxide composite. *Journal of Applied Polymer Science*, *107*, 1395–1400.

Khulbe, K. C., Kruczek, B., Chowdhury, C., Cacne, S., & Matsuura, T. (1996). Surface morphology of homogeneous and asymmetric membranes made from poly(pheny1ene oxide) by tapping mode atomic force microscope. *Journal of Applied Polymer Science*, *59*, 1151–1158.

Khurana, P., Aggarwal, S., Narula1, A. K., & Choudhary, V. (2003). Studies on the curing and thermal behaviour of DGEBA in the presence of bis(4-carboxyphenyl) dimethyl silane. *Polymer International*, *52*, 908–917.

Kim, H., & Macosko, C. W. (2009). Processing–property relationships of polycarbonate/graphene composites. *Polymer*, *50*, 3797–3809.

Liu, P. G., Gong, K. C., Xiao, P., & Xiao, M. (2000). Preparation and characterization of poly(vinyl acetate)-intercalated graphite oxide composite. *Journal of Materials Chemistry*, *10*, 933–935.

Matsuo, Y., Tahara, K., & Sugie, Y. (1997). Structure and thermal properties of poly(ethylene oxide)-intercalated graphite oxide. *Carbon*, *35*, 113–120.

Ma, X. F., Chang, P. R., Yang, J. W., & Yu, J. G. (2009). Preparation and properties of glycerol plasticized-pea starch/zinc oxide-starch bionanocomposites. *Carbohydrate Polymers*, *75*, 472–478.

Ma, X. F., Chang, P. R., Yu, J. G., & Stumborg, M. (2009). Properties of biodegradable citric acid-modified granular starch/thermoplastic pea starch composites. *Carbohydrate Polymers*, *75*, 1–8.

Ma, X. F., Yu, J. G., & Wang, N. (2008). Glycerol plasticized-starch/multiwall carbon nanotube composites for electroactive polymers. *Composites Science and Technology*, *68*, 268–273.

Metin, D., Tihminlioğlu, F., Balköse, D., & Ülkü, S. (2004). The effect of interfacial interactions on the mechanical properties of polypropylene/natural zeolite composites. *Composites: Part A*, *35*, 23–32.

Meyer, J. C., Geim, A. K., Katsnelson, M. I., Novoselov, K. S., Booth, T. J., & Roth, S. (2007). The structure of suspended graphene sheets. *Nature*, *446*, 60–63.

Ou, S. Y., Li, A. J., & Yang, A. H. (2001). A study on synthesis of starch ferulate and its biological properties. *Food Chemistry*, *74*, 91–95.

Park, S. J., & Kim, H. C. (2001). Thermal stability and toughening of epoxy resin with polysulfone resin. *Journal of Polymer Science Part B: Polymer Physics*, *39*, 121–128.

Ratnayake, W. S., Hoover, R., & Warkentin, T. (2002). Pea starch: Composition, structure and properties—A review. *Starch/Stärke*, *54*, 217–234.

Rehman, Z., & Shah, W. H. (2005). Thermal heat processing effects on antinutrients, protein and starch digestibility of food legumes. *Food Chemistry*, *91*, 327–331.

Schlemmer, D., Angélica, R. S., & Sales, M. J. A. (2010). Morphological and thermomechanical characterization of thermoplastic starch/montmorillonite nanocomposites. *Composite Structures*, *92*, 2066–2070.

Wang, G. X., Wang, B., Park, J., Yang, J., Shen, X. P., & Yao, J. N. (2009). Synthesis of enhanced hydrophilic and hydrophobic graphene oxide nanosheets by a solvothermal method. *Carbon*, *47*, 68–72.

Wang, S. J., Yu, J. L., & Gao, W. Y. (2005). Use of X-ray diffractometry (XRD) for identification of fritillaria according to geographical origin. *American Journal of Biochemistry and Biotechnology*, *1*, 207–211.

Wei, T., Luo, G., Fan, Z. J., Zheng, C., Yan, J., Yao, C. Z., et al. (2009). Preparation of graphene nanosheet/polymer composites using in situ reduction–extractive dispersion. *Carbon*, *47*, 2296–2299.

Wilhelma, H. M., Sierakowski, M. R., Souza, G. P., & Wypychc, F. (2003). Starch films reinforced with mineral clay. *Carbohydrate Polymers*, *52*, 101–110.

William, S., Hummers, J. R., & Richard, E. (1958). Preparation of graphitic oxide. *Journal of the American Chemical Society*, *80*, 1339.

Wu, J., Tang, Q., Sun, H., Lin, J., Ao, H., Huang, M., et al. (2008). Conducting film from graphite oxide nanoplatelets and poly(acrylic acid) by layer-by-layer self-assembly. *Langmuir*, *24*, 4800–4805.

Xu, Y. X., Hong, W. J., Bai, H., Li, C., & Shi, G. Q. (2009). Strong and ductile poly(vinyl alcohol)/graphene oxide composite films with a layered structure. *Carbon*, *47*, 3538–3543.

Xu, J. Y., Hu, Y., Song, L., Wang, Q. G., Fan, W. C., Liao, G. X, et al. (2001). Thermal analysis of poly(vinyl alcohol)/graphite oxide intercalated composites. *Polymer Degradation and Stability*, *73*, 29–31.

Yu, J. G., Yang, J. W., Liu, B. X., & Ma, X. F. (2009). Preparation and characterization of glycerol plasticized-pea starch/ZnO–carboxymethylcellulose sodium nanocomposites. *Bioresource Technology*, *100*, 2832–2841.